

2019

Argon Metastable and Resonant Level Densities in Ar and Ar/Cl² Discharges Used for the Processing of Bulk Niobium

Jeremy Peshl

Old Dominion University, jpeshl@odu.edu

Roderick McNeill

Old Dominion University, rmcne007@odu.edu

Charles I. Sukenik

Old Dominion University, csukenik@odu.edu

Milka Nikolić

Svetozar Popović

Old Dominion University, spopovic@odu.edu

See next page for additional authors

Follow this and additional works at: https://digitalcommons.odu.edu/physics_fac_pubs



Part of the [Atomic, Molecular and Optical Physics Commons](#), and the [Plasma and Beam Physics Commons](#)

Original Publication Citation

Peshl, J., McNeill, R., Sukenik, C. I., Nikolić, M., Popović, S., & Vůsković, L. (2019). Argon metastable and resonant level densities in Ar and Ar/Cl₂ discharges used for the processing of bulk niobium. *Journal of Applied Physics*, 126(10), 103302. doi:10.1063/1.5115043

This Article is brought to you for free and open access by the Physics at ODU Digital Commons. It has been accepted for inclusion in Physics Faculty Publications by an authorized administrator of ODU Digital Commons. For more information, please contact digitalcommons@odu.edu.






Authors

Jeremy Peshl, Roderick McNeill, Charles I. Sukenik, Milka Nikolić, Svetozar Popović, and Leposava Vůsković

Argon metastable and resonant level densities in Ar and Ar/Cl₂ discharges used for the processing of bulk niobium

Cite as: J. Appl. Phys. **126**, 103302 (2019); <https://doi.org/10.1063/1.5115043>

Submitted: 18 June 2019 . Accepted: 22 August 2019 . Published Online: 09 September 2019

Jeremy Peshl , Roderick McNeill , Charles I. Sukenik , Milka Nikolić , Svetozar Popović , and Leposava Vůsković



View Online



Export Citation



CrossMark

ARTICLES YOU MAY BE INTERESTED IN

One-dimensional multiperiodic photonic structures: A new route in photonics (four-component media)

Journal of Applied Physics **126**, 103102 (2019); <https://doi.org/10.1063/1.5115829>

In situ dynamic transmission electron microscopy characterization of liquid-mediated crystallization of amorphous Ge

Journal of Applied Physics **126**, 105110 (2019); <https://doi.org/10.1063/1.5117845>

Photoinduced valence tautomerism of a cobalt-dioxolene complex revealed with femtosecond M-edge XANES

The Journal of Chemical Physics **151**, 104201 (2019); <https://doi.org/10.1063/1.5115227>

Lock-in Amplifiers
... and more, from DC to 600 MHz



Argon metastable and resonant level densities in Ar and Ar/Cl₂ discharges used for the processing of bulk niobium

Cite as: J. Appl. Phys. **126**, 103302 (2019); doi: [10.1063/1.5115043](https://doi.org/10.1063/1.5115043)

Submitted: 18 June 2019 · Accepted: 22 August 2019 ·

Published Online: 9 September 2019



Jeremy Peshl,^{1,a)} Roderick McNeill,¹ Charles I. Sukenik,¹ Milka Nikolić,² Svetozar Popović,¹ and Leposava Vusković¹

AFFILIATIONS

¹Department of Physics, Old Dominion University, Norfolk, Virginia 23529, USA

²Department of Physics and Astronomy, University of San Francisco, San Francisco, California 94117, USA

^{a)}Electronic mail: jpeshl@odu.edu

ABSTRACT

A comparative analysis of two popular spectroscopy techniques is conducted in a coaxial cylindrical capacitively coupled discharge designed for the plasma processing of superconducting radio frequency (SRF) cavities. The density of the metastable and resonant levels in Ar is measured in both Ar and Ar/Cl₂ discharges to properly characterize the unique discharge system and aid in the development of a cavity etching routine. The first method, deemed the “branching fraction method,” utilizes the sensitivity of photon reabsorption of radiative decay to measure the lower state (metastable and resonant) densities by taking ratios of spectral lines with a common upper level. This method has been gaining popularity as it does not require any *a priori* knowledge about the electron energy distribution. The second method is a tunable diode laser absorption spectroscopy technique that measures the thermal Doppler broadening of spectral lines, from which the neutral gas temperature and lower state density of the transition can be evaluated. The two methods were conducted in tandem, while external parameters that were empirically determined to be important to the etching mechanism of SRF cavities are varied. Relationships between the excited state densities and the external parameters are presented for both spectroscopy methods and conclusions about the effects of these parameters on the discharge are stated when appropriate.

Published under license by AIP Publishing. <https://doi.org/10.1063/1.5115043>

I. INTRODUCTION

Metastable and resonant states of excited Ar atoms play an indirect but important role in the interaction of rf discharges with solid surfaces. One aspect of this interaction, in general, is the direct or indirect role in the ion assisted reactive ion etching (IARIE) of metallic surfaces in increasing the population of both assisting and reactive ions, modification of the electron energy distribution function (EEDF), and in the chemical kinetics of the etching process.^{1,2} Ionized mixtures of reactive and noble gases are the natural medium for IARIE, and their application to chemical kinetics is not very well documented. This situation affects the understanding of surface phenomena of practical interest in the processing of large metallic surfaces, such as the rate of material removal, surface roughness, and electron field emission from nano-scale particulates.

IARIE techniques have entered competitively into the development of resonant superconductive radio-frequency (SRF) niobium (Nb) cavities used in high energy particle accelerators.^{3–9} The aim is to complement or replace the “wet” acid processes that are commonly used to remove surface impurities that limit the performance of the bulk superconductive medium and to create a smooth surface with the reduction of grain boundaries and pits.¹⁰ By adopting the same basic principles used on the semiconductor nanotechnology, IARIE shows promise in the preparation of SRF cavities for use in particle accelerators by potentially achieving similar or better superconducting properties as compared to current methods while decreasing costs, processing time, and manpower.

Much of the work done in the adaptation of the IARIE technology to SRF cavities has been to prove that this process is viable and controllable for etching concave cylindrical surfaces.^{3–9} While it has

shown some success, the work has left significant information missing about the plasma parameters and dynamics within the etching reactor. The plasma etch process uses a mixture of Ar and Cl_2 (85%/15%) to remove surface layers from bulk Nb. Ar/ Cl_2 mixtures are commonly used for etching polysilicon, but characterizing the plasma chemistry remains elusive as the discharge is inherently electronegative. The addition of another negative species (Cl^- ions) makes particle and energy balance analysis difficult, as the theoretical description of the discharge is much more complicated.¹¹ Conversely, electropositive pure Ar discharges have been extensively studied.^{12–21} Furthermore, the radial cross section of the accelerating SRF cavity inner surface is elliptic, which complicates the characterization of the discharge and direct comparisons to a simpler planar geometry cannot be made. The coaxial configuration used for cavity etching is an asymmetric discharge due to the different surface areas of the two electrodes. This is unfavorable for the etching of the larger electrode due to the large negative self-bias voltage on the smaller powered electrode. The discharge asymmetry is, therefore, reversed with a positive dc bias and a corrugated inner electrode.⁶ In order to reduce the complex reactor geometry and make the discharge more suitable for characterization, without affecting the plasma parameter distribution, a three-step transformation had to be made to simplify the reactor into a closed cylinder-to-disc generic electrode configuration that could support spectroscopic observations.

This work uses optical absorption and emission spectroscopy to measure plasma properties of the discharge. Quantities like electron density, electron temperature, ion and neutral densities can be evaluated from the recorded spectra. The densities of Argon's first four excited states in Ar and Ar/ Cl_2 discharges are among those with particular importance. These include the two resonant ($1s_2$ and $1s_4$ in the Paschen notation) and two metastable ($1s_3$ and $1s_5$) levels. The two long-lived metastable levels, with a relatively large stored energy, have a strong influence on the excitation and chemical processes. One of the main goals of this paper is to inspect a possible influence of these states on the etching chemistry.

A significant goal of this work is to explore the spectroscopic technique now known as the optical emission spectroscopy-branching fraction method (OES-BFM).^{12,17,22,23,32} This technique uses the intensities of partially self-absorbed spectral emission lines from $2p \rightarrow 1s$ transitions to determine the amount of reabsorbed photons (the photon escape factor). This optical emission spectroscopy technique is essentially nonintrusive and dependent on the distribution of the lower state density of the transition. A set of simultaneously recorded line intensity pairs is chosen so that they involve densities of all $1s$ states from a single broad range calibrated spectrum. Ratios of the escape factors (or modified branching fractions) of those lines with densities as free parameters are adjusted to the ratios of recorded spectral lines. Thus, the whole set of $1s$ densities at a particular location is obtained from a single emission spectrum in the 650–1000 nm range.

The OES-BFM technique is compared to tunable diode laser absorption spectroscopy (TDLAS) to obtain directly the absorption coefficient of a single transition $1s \rightarrow 2p$.^{22–25} The Doppler broadened line profile allows one to evaluate the kinetic gas temperature of atoms in the particular $1s$ state. This value is necessary in all evaluations of the absorption coefficients for all transitions involved in the two techniques.

This paper is organized as follows. In Sec. II, the two techniques for evaluating the $1s$ densities are reviewed separately and discussed. The analysis includes the cross-reference between the two techniques. In Sec. III, we describe the experimental chamber, equipment used, and method of the observation for both techniques. Section IV contains results pertaining to the neutral gas temperature measured using TDLAS for both Ar and Ar/ Cl_2 discharges. In Sec. V, we present the experimental results in the form of the density dependence upon external discharge parameters. Furthermore, we discuss comparatively the values and uncertainties of $1s$ densities obtained with the two techniques and interpret the results in terms of the plasma kinetics and the consequences thereof. Section VI contains a short discussion of the significant effects of dc bias on the discharge, particularly as it pertains to etching. In Sec. VII, we underline a general overview of the results of this work.

II. EVALUATION METHODS OF Ar $1s$ STATE DENSITIES

The significant advantage of using optical diagnostic methods is the nonintrusive nature of these measurements, while Langmuir probes have a direct influence on the discharge. Line ratio techniques utilizing the transitions of the first 14 excited states of Ar are popular, but many require prior knowledge of the electron energy distribution function (EEDF) and collisional cross sections. The line ratio technique used in this study is based on the work by Schulze *et al.*¹² and does not require any prior knowledge about the discharge, and thus, can be used without needing to make a great deal of assumptions. This method is still rather new and its validity needs to be tested for a variety of discharge configurations.

In order to properly use OES-BFM, the gas temperature (T_g) of the discharge must be known, as is explained in Subsection II A. Oftentimes, this can simply be approximated as it does not have a drastic effect on the final values of the densities. However, since a coaxial cylindrical capacitively coupled plasma (CCP) is not a typical discharge chamber, a direct measurement of T_g was necessary. This is commonly done by using a tunable diode laser to measure the Doppler broadening of a $2p \rightarrow 1s$ spectral line and fitting the corresponding signal to a Gaussian. The full width half maximum (FWHM) of the Gaussian profile can be used to calculate the corresponding T_g . However, this measurement has the added benefit of additionally providing a way to calculate the lower state density of the measured transition line with no additional experimental cost. Therefore, the densities measured by the two spectroscopic methods can be compared depending on the transitions that can be measured by the tunable laser. In this work, we used a laser diode tunable to transitions at 810.37 nm and 811.53 nm to excite the $1s_4 \rightarrow 2p_7$ and $1s_5 \rightarrow 2p_9$ transitions, respectively, thereby allowing the measurement of the $1s_4$ and $1s_5$ level densities. The mathematical details of the two methods are given below.

A. OES-branching fraction method

Assuming a homogeneous distribution of excited atoms and excitation sources in the bulk of the cylindrical capacitive discharge, the spectral line intensity of a transition $i \rightarrow j$ as recorded with a

detector can be expressed as

$$\bar{I}_{ij} = c\gamma_{ij}(n_j)A_{ij}n_i, \quad (1)$$

where \bar{I}_{ij} is the line of sight averaged spectral line irradiance from a given observation column, c is a constant which defines the geometry of the observation column, $\gamma_{ij}(n_j)$ is the radiation-reducing Holstein's²⁶ escape factor, n_j is the average density of atoms in the lower, 1s state, A_{ij} is the transition probability, and n_i is the density of atoms in the upper, 2p state. The use of the line irradiance from rf discharges avoids the effect of Doppler, instrumental, and Stark broadening. The irradiance depends on the densities of both states in the transition and increases with the density of emitters, n_i (2p state), and decreases with the density of absorbers, n_j (1s state). Therefore, there are two unknown variables in the nonlinear equation (1) for every 2p→1s transition. In the branching fraction method, the irradiances from a pair of 2p→1s transitions with the same upper level are divided to eliminate the density of the 2p state and the geometric factor. This leads to^{12,17,22}

$$\frac{\bar{I}_{ij}A_{ik}}{\bar{I}_{ik}A_{ij}} - \frac{\gamma_{ij}(n_j)}{\gamma_{ik}(n_k)} = 0, \quad (2)$$

where the ratio of irradiances is measured, the ratio of transition probabilities are known, and the ratio of escape factors depends on the unknown densities of the corresponding two 1s states, which have to satisfy Eq. (2). The escape factor in its most accurate form is evaluated from the integral of the photon transmission coefficient over the plasma volume and is dependent on the distribution of emitters and absorbers along the observation column.^{26–28} A more complete investigation of the photon escape factor and its application to low temperature plasmas can be seen in the work by Zhu *et al.*²⁹ There are, however, several approximations that can be used in measurements with various levels of accuracy.^{22,26,30–32} For this work, we follow the case of a homogeneous distribution of emitters and absorbers proposed by Mewe,^{30,31}

$$\gamma_{ij} = \frac{2 - \exp(-\tau_{ij}/1000)}{1 + \tau_{ij}}, \quad \tau_{ij} = k_{ij}l, \quad (3)$$

where τ_{ij} is the optical thickness of the observed plasma column at the center of the spectral line corresponding the $i \rightarrow j$ transition.³¹ The value l is the effective plasma length defined as the radius of the cylindrical plasma for a volume averaged escape factor.²⁹ In this work, this is equivalent to the radius of the discharge chamber. The reabsorption coefficient $k_{ij}(n_j)$ is given by

$$k_{ij}(n_j) = \frac{\lambda_{ij}^3}{8\pi^{3/2}} \frac{g_i}{g_j} A_{ij} n_j \sqrt{\frac{M}{2k_B T_g}} = \alpha_{ij} n_j, \quad (4)$$

where λ_{ij} is the center wavelength of the transition, g_i and g_j are the statistical weights of the the upper and lower states, respectively, M is the atomic mass, k_B is the Boltzmann constant, and T_g is the gas

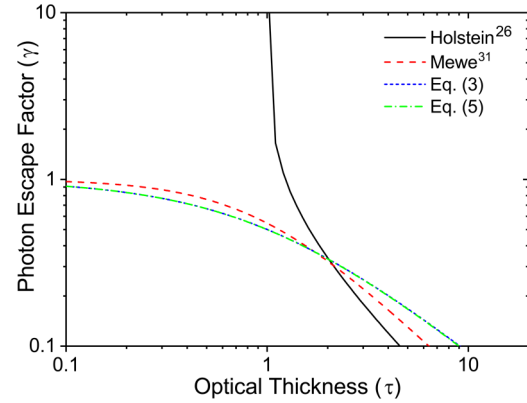


FIG. 1. Various forms of the photon escape factor as a function of optical thickness found in the literature.

temperature. All known quantities are grouped in α_{ij} , which is calculated for every measured spectral line.

For the range of densities found in capacitive discharges, an even more simplified version of the escape factor was used,²²

$$\gamma_{ij} \approx \frac{1}{1 + \tau_{ij}}. \quad (5)$$

Figure 1 shows the escape factor values evaluated from Refs. 22, 26, 30, and 31 plotted against the optical thickness corresponding to the lower state density range of 10^{15} – 10^{18} m⁻³. The escape factor values are distributed over two orders of magnitude, depending on the approximation. The difference between Eqs. (3) and (5) is negligible in the optical thickness range of this work as outlined in Fig. 1. Within the conditions of this experiment, we have deemed that Eq. (5) is sufficient for our purposes.

The densities of the four Ar 1s states can be evaluated using Eq. (2). The density of atoms at each level was calculated using a nonlinear least square method to minimize the sum of a set of five transition pairs

$$\sum_{m=1}^5 \left[\left(\frac{I_1 A_2}{I_2 A_1} \right)_m - \left(\frac{\gamma_1}{\gamma_2} \right)_m \right]^2. \quad (6)$$

The Ar 1s densities (and, therefore, the photon escape factors) were iteratively adjusted so that the above sum is minimized below 1%. With four unknowns (the 1s state densities), five density pairs are used as in Ref. 12 to overconstrain the system and reduce errors.

B. Tunable diode laser absorption spectroscopy

Using an external light source emitting at a wavelength of a transition $1s_j \rightarrow 2p_i$ in a discharge, one can measure the absorption of this light and determine the density of the absorbing $1s_j$ states. Provided that the absorbers are uniformly distributed in the discharge, the intensity of transmitted light is described by the

Beer-Lambert law as

$$I(\nu) = I_0(\nu)e^{-k_{ij}(n_j)l}, \quad (7)$$

where ν is the frequency of the transmitted light, $I(\nu)$ is the intensity of the incident light, l is the length of the observation column (equal to the diameter of the plasma cylinder), and $k_{ij}(n_j)$ is the absorption coefficient of the $1s_j \rightarrow 2p_i$ transition. As defined in Eq. (3), $k_{ij}(n_j)l = \tau_{ij}(\nu)$ is the optical thickness. Frequency and wavelength domains are conveniently interchanged in the case of narrow incident light and a narrow line profile, which is interrogated by scanning the incident light about the line center in the frequency domain and recording the transmitted intensity. The incident light was provided by a laser diode tunable around the center of the absorption line. The transmitted and incident intensities are defined by four distinct measurements, required for each scan,

$$I(\nu) = L(\nu) - P(\nu), \quad (8a)$$

$$I_0(\nu) = L_0(\nu) - B(\nu), \quad (8b)$$

where $L(\nu)$ is the detected intensity when both the discharge and laser is on, $P(\nu)$ is the detected intensity when the discharge is on and the laser is off, $L_0(\nu)$ is the detected intensity when the discharge is off and the laser is on, and $B(\nu)$ is the detected intensity when both the discharge and laser are off.

The absorption line profile is dominated by the Doppler broadening due to the kinetic motion of absorbers. The Doppler broadening is the only significant broadening mechanism for the parameters of this work. The typical line profile is 800–900 MHz, while Stark and natural broadening are of the order of tens of megahertz. The absorption coefficient has the general form^{12,17,23–26,33}

$$k_{ij}(\Delta\nu) = \frac{\lambda_{ij}^2}{8\pi} P_{ij}(\Delta\nu) \frac{g_i}{g_j} n_j A_{ij}, \quad (9)$$

where $\Delta\nu = \nu - \nu_0$ and ν_0 is the central frequency of the transition line, and $P_{ij}(\Delta\nu)$ is the Doppler broadened (Gaussian) line profile^{12,23,26}

$$P_{ij}(\Delta\nu) = P_0(\lambda_{ij})e^{-[P_0(\lambda_{ij})\Delta\nu]^2}, \quad (10a)$$

$$P_0(\lambda_{ij}) = \lambda_{ij} \sqrt{\frac{M}{2\pi k_B T_g}}. \quad (10b)$$

In the first step of this method, the full width of the scanned absorption profile at half maximum, $\Delta\nu(\text{FWHM})$, is measured and

the gas temperature is evaluated from^{23–25,33}

$$T_g = \frac{M}{2k_B \ln(2)} \left(\frac{\lambda_{ij} \Delta\nu_D(\text{FWHM})}{2} \right)^2. \quad (11)$$

In the second step, the lower state density n_j is evaluated by using the Beer-Lambert law from the full absorption coefficient of the state j ,^{23,25,33}

$$\int_0^\infty \ln \left(\frac{I_0(\nu)}{I(\nu)} \right) d\nu = S = \frac{\lambda_{ij}^3 A_{ij} n_j g_i}{8\pi^{3/2} g_j} l \sqrt{\frac{M}{2k_B T_g}}, \quad (12)$$

where S is the area of the Gaussian spectral profile.

III. EXPERIMENTAL SETUP

A. Discharge chamber and experimental conditions

The experimental setup closely resembles that of the previous work reported by Upadhyay *et al.*^{3–9} The main differences are upgrades in the pumping system. The plasma chamber is evacuated using a combination of a Pfeiffer/Adixen ATH-500MT turbomolecular pump and a Leybold Trivac D65 BCS PFPE rough pump. Since the apparatus is so large and long, the pressure is monitored by two Agilent FRG-700 Pirani gauges at either end of the experiment, both upstream and downstream of the gas flow. The pressure of the plasma processing area is then calculated to be the average of these two readings.

A schematic of the modular discharge chamber is shown in Fig. 2. The chamber is a stainless steel cylinder with eight miniconflat ports extending from the sides. The cavity has a length of 26.5 cm and a diameter of 10.0 cm. The powered electrode has a corrugated structure and is made of niobium with a length of 8.2 cm and a diameter of 5.1 cm.⁶ The corrugated structure is used to increase the surface area and help with the reversal of the plasma asymmetry to aid in etching the surface of the cavity/chamber.⁶ The discharge gases (either Ar or Ar/Cl₂) are fed into the chamber through a Nb conical showerhead to ensure that the gas is distributed evenly. The conical gas inlet was biased to the same positive dc voltage as the powered electrode to avoid etching of the showerhead.

In order to properly characterize both Ar and Ar/Cl₂ discharges in this configuration, each potentially important external parameter must be studied independently. The array of external parameters was empirically established in previous work for the best etching outcome, with the Nb etch rate between 60 and 200 nm/min for the range of these parameters in this work.^{3–7,9} A summary of external parameters is given in Table I. In particular, the effect of dc bias on the $1s$ densities and gas temperature is important as it is necessary for the etching of bulk niobium, but there is little known information about its effect on these plasma parameters.

It is important to clarify the given values for the dc bias parameter as it can easily be misconstrued. Self-bias refers to the powered electrode having no positive bias added to the electrode, so it only has the negative self-bias that develops due to the plasma

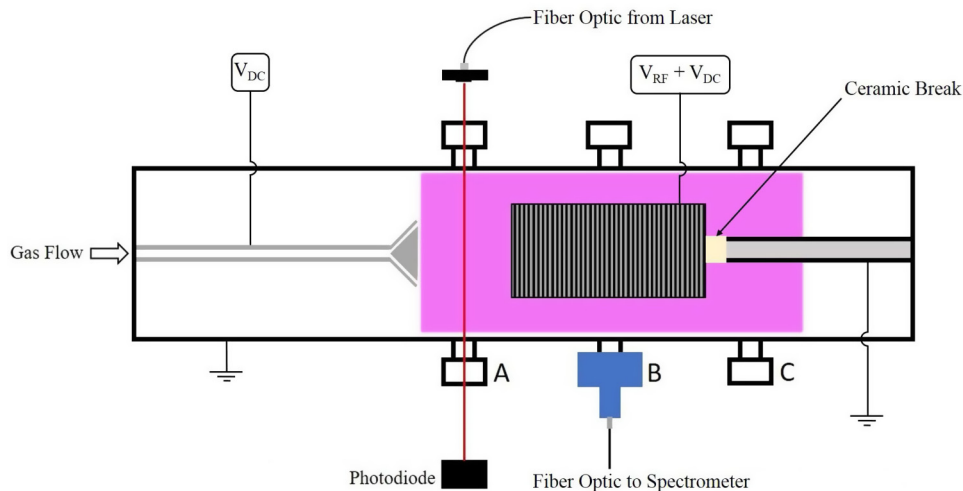


FIG. 2. Sketch of the discharge chamber. Spectral measurements can be taken in positions A, B, and C, although only measurements from position A are presented in this work. The laser is blocked for spectral measurements in position A.

asymmetry. The other values indicate a total dc bias (self-bias + added bias) of 0 V, 50 V, or 100 V. For example, a dc bias of 50 V indicates that a positive bias has been added to the powered electrode to bring the total bias to +50 V. The self-bias on the powered electrode will change depending on the experimental conditions, and, therefore, the amount of external bias that needs to be applied to reach these values will change accordingly. Throughout this work, the absolute value of the self-bias is not used or quoted to more effectively present results. This is because, as will become evident, the transition from “negative” total bias to “positive” total bias is seemingly more important than the “magnitude” of the total bias. The dc power supply used for providing the external bias is single sided, meaning that effects of an external bias can only be measured at values ≥ 0 V. This is not a problem for etching but is a limitation in the scope of this work.

B. Optical methods

1. Setup: OES-branching fraction method

The emission spectra are measured using an Ocean Optics HR4000CG-UV-NIR spectrometer, capable of measuring spectral lines from 200 to 1100 nm in a single scan with a 1 nm resolution. The spectrometer was calibrated using an Oriel Quartz-Tungsten Halogen blackbody lamp source (Model No. 63358). A 600 micron fiber (OceanOptics P600-5-VIS-NIR) was used for each measurement along with a 3D printed aperture to limit the acceptance

angle of the fiber optic, as well as ensure the fiber took measurements in a consistent line of sight through the plasma chamber. The fiber optic has a natural acceptance angle of 15° in all directions, and the aperture limits this acceptance angle to below 5° , allowing for a more accurate line of sight measurement. The mini-conflat ports allow for spectral measurements at various locations in the chamber; however, only results measured from position A are discussed here.

An example of an optical emission scan used for OES-BFM can be seen in Fig. 3 and the transitions used for this analysis are outlined in Table II. The spectral lines of interest are all within the 650–900 nm range and are paired as follows: 696.54/826.45 (n_{1s5}/n_{1s2}), 840.82/738.40 (n_{1s2}/n_{1s4}), 738.40/706.72 (n_{1s4}/n_{1s5}), 706.72/840.82 (n_{1s5}/n_{1s2}), and 852.14/794.82 (n_{1s2}/n_{1s3}). Using five ratios overconstrains the system and allows for a further reduction in errors. The 727.29 nm line was considered for the analysis, but

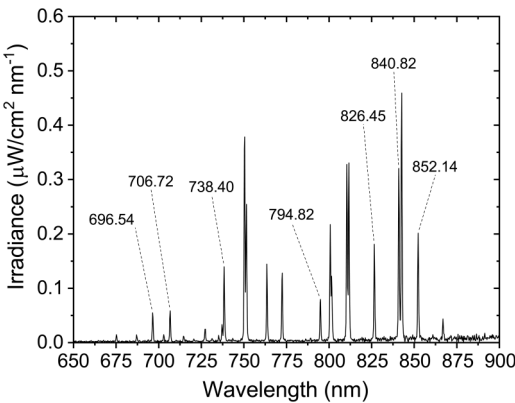


FIG. 3. Example of optical emission spectra of an Ar discharge. The signal has been calibrated and data are in units of irradiance. Pertinent transitions are outlined in Table II.

TABLE I. The external parameters studied. The * indicates that these values are not present for all data sets due to experimental limitations.

Parameter	Value	Unit
Pressure	10*, 25, 50, 75, 100*	mTorr
f power	25, 50*, 75, 100*, 150	W
dc bias	Self-bias, 0, 50, 100	V
Cl ₂ concentration	0, 1, 5, 10, 15*	%

TABLE II. Atomic data of argon transitions used in this work.³⁴

λ (nm)	Paschen	Russell-Saunders	$g_i - g_j$	A_{ij} (s^{-1})
826.45	$2p_2 \rightarrow 1s_2$	$4p'[1/2]_1 \rightarrow 4s'[1/2]_1$	3 - 3	1.53×10^7
696.54	$2p_2 \rightarrow 1s_5$	$4p'[1/2]_1 \rightarrow 4s'[3/2]_2$	3 - 5	6.40×10^6
840.82	$2p_3 \rightarrow 1s_2$	$4p'[3/2]_2 \rightarrow 4s'[1/2]_1$	5 - 3	2.23×10^7
738.40	$2p_3 \rightarrow 1s_4$	$4p'[3/2]_2 \rightarrow 4s'[3/2]_1$	5 - 3	8.50×10^6
706.72	$2p_3 \rightarrow 1s_5$	$4p'[3/2]_2 \rightarrow 4s'[3/2]_2$	5 - 5	3.80×10^6
852.14	$2p_4 \rightarrow 1s_2$	$4p'[3/2]_1 \rightarrow 4s'[1/2]_1$	3 - 1	1.39×10^7
794.82	$2p_4 \rightarrow 1s_3$	$4p'[3/2]_1 \rightarrow 4s'[1/2]_0$	3 - 1	1.86×10^7

the low intensity of the line prevented it from being useful in the system of equations. Once the spectral lines are measured, they are fit to a Gaussian and integrated using the Origin fitting software. The resulting integrated value for each peak, which is in units of radiance ($\mu W/cm^2$), is used for the reduction of Eq. (6). The expected and calculated error for OES-BFM is higher due to the low resolution of the spectrometer, the extended calibration required, and the acceptance angle of the fiber. The error for each measurement was calculated from standard error calculations of two sets of measurements taken on separate days under the same conditions. Data points that do not have multiple measurements for those specific conditions due to experimental errors are given a statistical error of 30% as a default.

2. Setup: Tunable diode laser absorption spectroscopy

An external cavity diode laser was built using a 150 mW Sanyo semiconductor diode with a nominal free running wavelength of 808 nm in a Littman-Metcalf configuration.³⁵ This laser was capable of scanning both the 810.37 nm and 811.53 nm transition lines after proper tuning to measure the gas temperature and the $1s_4$ resonant and $1s_5$ metastable level densities. The laser can be tuned to a transition by a coarse adjustment of the grating in the cavity, along with temperature and laser current adjustments. Once the laser is tuned to a transition, the laser is able to scan over the line by using a piezoelectric device to adjust the mirror in the

cavity by small amounts. In addition, a feed-forward circuit, which allows the current to be adjusted simultaneously with the piezoelectric, was built to increase the scanning capabilities of the laser. The feed-forward circuit was built based on a simpler version of the design by Doret.³⁶ The combination of the piezoelectric and feed-forward allowed for a mode-hop free scan of 4 GHz, which is more than sufficient with an expected ν (FWHM) of approximately 1 GHz.

The laser is guided through an optical isolator into a beam splitter that allows a portion of the beam to be sent to two different Fabry-Pérot Interferometers (FPIs). One is a ThorLabs SA200-7A with 1.5 GHz Free Spectral Range (FSR), and the other is a homemade low finesse parallel mirror interferometer with a calibrated FSR of 303 MHz. Due to the piezoelectric and feed-forward circuit required to get the laser to sweep over a large enough frequency range, the resulting scan signal has a nonlinear scan rate that propagates throughout the scan. Since the laser can only scan 4 GHz mode-hop free, the 1.5 GHz FSR of the ThorLabs is too large to properly detect and account for this nonlinearity. The lower FSR of the homemade interferometer allows for this nonlinearity to be seen over the length of the scan, and the scan can be calibrated accordingly.

The other half of the beam is then split again to be sent to a low pressure Ar reference discharge cell for wavelength confirmation and laser tuning. The other part of the beam is sent to a flip mount that can either send the beam to a Burleigh WA-20VIS wavemeter or to a fiber launcher which sends the beam to the plasma chamber. The laser is sent through an unobstructed area of the plasma chamber in front of the powered electrode by passing through two miniconflat ports. The beam is collected on the other side of the chamber by a ThorLabs DET100A photodiode and sent to a 4-channel oscilloscope that measures the laser absorption, the two FPIs, and the piezoelectric voltage signal (which shows the bounds of the scan).

Using the Beer-Lambert law, the absorption signal is converted into the signal shown in Fig. 4 and fit to a Gaussian. The resulting Gaussian fit yields all the pertinent information to calculate the gas temperature and density.

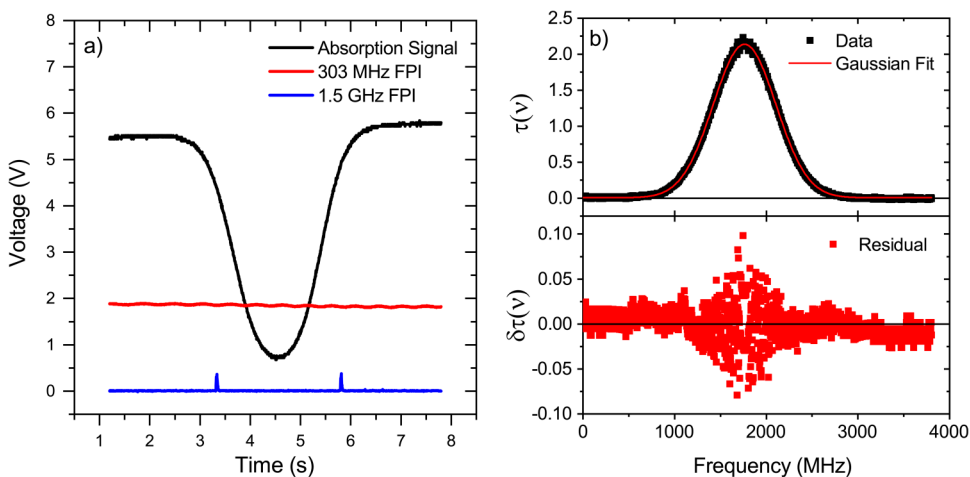


FIG. 4. Example of laser absorption measurement using TDLAS: (a) laser absorption and two Fabry-Pérot Interferometer signals (the piezo voltage signal is not pictured); (b) the processed signal along with the residual plot.

Each measurement consisted of three scans, which were fit and then averaged, to ensure that the scans are consistent and reliable. The error in TDLAS measurements is calculated from a combination of the error in the Gaussian fits of the profile and the frequency calibration. The error in these measurements is very small compared to OES-BFM with an average error of $\pm 3\%$.

C. Comparison of TDLAS and OES-BFM

A significant motivation for this work is to validate the feasibility of using OES-BFM to accurately measure the Ar 1s densities in Ar and Ar/Cl₂ discharges. Based on published work, there is no reason *a priori* as to why it could not be used in the cylindrical capacitively coupled plasma (CCP) discharge, but as this system is distinctly unique, and since there are no published works to directly compare, the OES-BFM results must be compared to a more accurate method of measurement. Therefore, the densities evaluated from OES-BFM are compared to those measured from TDLAS. Since TDLAS has the distinct disadvantage of only being able to measure one transition at a time, and the need for a laser that can be tuned to particular wavelengths, only certain densities could be compared. However, the closeness of the 810.37 nm and 811.53 nm lines allow for a measurement of both the Ar 1s₄ and 1s₅ densities with the same tunable laser. OES-BFM has the advantage of being able to calculate all four lower level densities simultaneously by using an array of measured spectral lines from a low resolution, high speed spectrometer.

In general, a direct comparison of densities measured using TDLAS and OES-BFM shows consistency within a factor of eight, with the largest discrepancy stemming from the measurements conducted at lower pressures, most prominently those at 10 mTorr. At 25 mTorr and above, TDLAS and OES-BFM are consistent within a factor of three for all measured parameters, with a vast majority of those results well within a factor of two. Published work outlining OES-BFM in comparison to TDLAS or other experimentally measured results show consistency usually within a factor of two.^{17,22} Indeed, Li *et al.* have shown significant improvements of OES-BFM results with the use of a monodirectional escape factor instead of the volume averaged escape factor commonly associated with this method.³² While this is a promising modification to the method, we have elected to remain consistent to the original technique and explore the use of a monodirectional escape factor in future work. As it stands, the results are sufficiently consistent to make significant qualitative observations, as both sets of measurements vary similarly as a function of external parameters. This is particularly true for results pertaining to the Ar 1s₅ densities as they are more consistent than the 1s₄ densities as a whole. These observations are pointed out throughout the analysis to provide an argument of OES-BFM as a reliable diagnostic technique.

While OES-BFM is a fast and convenient method, it has a number of limitations that are being discovered as attempts are made to extend this technique to different types of systems, particularly in mixed Ar discharges. It was the goal of this work to use OES-BFM in Ar/Cl₂ discharges, but there was little to no success. The limitations and proposed reasons why this technique is not effective in Ar/Cl₂ discharges is discussed in Subsection III D.

D. Limitations of OES-BFM

In principle, OES-BFM should work as long as there are enough metastable atoms to produce measurable changes in the effective branching fraction (for more information on the effective branching fraction, see Ref. 18). With that being said, the method can fail if there are not enough metastables in the discharge or if the changes in the branching fractions due to reabsorption cannot be measured. In the case of this work, there is most likely a combination of both of these problems. Metastable level densities measured using TDLAS show a drop of upwards of two orders of magnitude when Cl₂ is added to the discharge, depending on the concentration. This is not unexpected as the addition of another species, especially one that creates an electronegative discharge, would reduce the energy and collisions required to populate Ar metastables. In addition, the quenching rate of Ar metastables due to Cl₂ is rather high at $71 \times 10^{17} \text{ m}^3/\text{s}$.³⁷ For context, this is about twenty times higher than N₂ and three times higher than O₂, two other common plasma discharge additives.³⁷ Wang *et al.* has shown that OES-BFM can be effective in a 15 mTorr Ar/O₂ inductively coupled plasma (ICP) discharge in concentrations up to 50%.³⁸ For our case, the partial pressure of Cl₂ in our discharge is comparable to Wang's for many of our measurements, particularly those that are closest to previously established etching conditions (15% Cl₂ at 50 mTorr). The combination of high partial pressures and the metastable-Cl₂ quenching rate makes OES-BFM a difficult measurement technique for the Ar/Cl₂ discharge. At those conditions in which the partial pressure was very small (1% concentration of Cl₂) OES-BFM managed to produce some reasonable results, but not enough to make clear conclusions.

The necessity of having enough metastable atoms to modify the effective branching fraction naturally leads to an investigation of the lower limit of the density in which OES-BFM can be useful. This is not easy to estimate, but the limitations can be illuminated by considering the form of the photon escape factors for the transitions used in the analysis. A plot of the photon escape factor for a number of spectral lines used in the analysis is shown in Fig. 5.

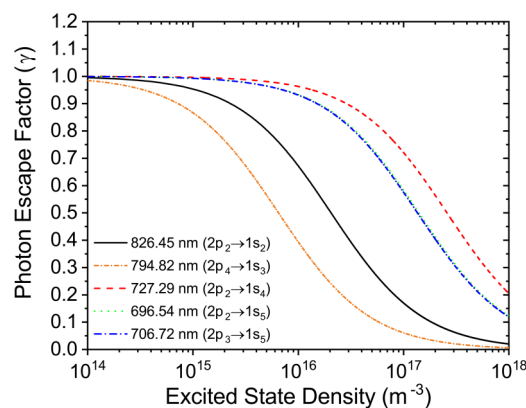


FIG. 5. Calculated photon escape factors using Eq. (5) vs Ar 1s population density.

Figure 5 shows that below 10^{16} m^{-3} , the change in the photon escape factor for transitions involving the Ar $1s_5$ metastable level is quite small compared to the other transitions. Below 10^{15} m^{-3} , the photon escape factor is approximately 1 for all transitions. In addition, it is pertinent to point out that for the condition of this discharge the Ar $1s_5$ density is consistently the highest of the four $1s$ levels, sometimes by almost an order of magnitude. Therefore, even if the Ar $1s_5$ density is in the low to mid 10^{16} m^{-3} , the other densities may be so much lower that OES-BFM cannot properly work. The combination of these two issues better explains the reason why realistic results for Ar/Cl₂ discharges were seemingly unattainable.

IV. GAS TEMPERATURE

The gas temperature is a necessary quantity for OES-BFM, and it was measured for the array of external parameters outlined in Sec. III. Overall, the gas temperature did not vary significantly as a function of the external parameters. In a pure Ar discharge, the gas temperature is consistently in the 370–420 K range with only a few instances of T_g dropping below 370 K. The average gas temperature for the Ar discharge across all external parameters is $391 (\pm 15) \text{ K}$, which was rounded up to 400 K for all calculations presented here. This value for T_g is lower than the temperature in analogous works, but those experimental configurations use inductively coupled plasmas in a much smaller configuration.^{17,12,25} Sushkov *et al.*²² conducted similar OES-BFM/TDLAS measurements in a parallel-plate CCP and measured T_g in the range of 320–410 K, which closely matches the T_g range of this work and has the most similar experimental conditions.²²

The Ar/Cl₂ discharge has a larger range of measured values, but, in general, T_g remained between 350 and 450 K. Once again, for ease of use in the OES-BFM data analysis program, the gas temperature was approximated to 400 K since the average T_g across all external parameters is $423 (\pm 24) \text{ K}$. The gas temperature has been measured previously for Cl₂ containing plasmas and typically show an increase in T_g as the rf power is increased.³⁹ However, this is once again an ICP reactor with much higher rf power upper limits, so we are confident that the values found for T_g in this work are appropriate.

V. RESULTS

We present the $1s_4$ and $1s_5$ excited state densities of Ar in both Ar and Ar/Cl₂ discharges as a function of external parameters. As stated in Sec. III, the range of external parameters is defined based on empirical results of previous etching experiments. Statistical error bars are included on all presented plots, however the error is oftentimes smaller than the plot symbol size. The $1s_2$ and $1s_3$ densities are not presented here, but on average we have seen $n_{1s4} \approx 3n_{1s2}$ and $n_{1s5} \approx 6n_{1s3}$. Due to the limitations outlined in Sec. III D, all presented results involving Ar/Cl₂ discharges were measured using TDLAS.

A. Pressure

1. Ar discharge

The effects of increasing pressure on the $1s_4$ and $1s_5$ levels are well established in the literature, particularly for rf ICPs in pure Ar.^{17,12,25,40} In general, there is an initial increase in both density populations as pressure is increased, with an eventual plateau and decrease as pressure is increased further. This effect can be explained in terms of the dominant creation and loss mechanisms of the excited levels in the discharge. At lower pressures, the metastable atoms are primarily lost to diffusive and collisional losses to the resonant levels, while the resonant density is mainly lost to radiative decay to the ground state. An increase in pressure facilitates an increase in the electron density, which leads to an increase in the excited state density as more electron-atom excitation collisions take place. Eventually, the electron density reaches a point where decay from electron-atom collisions (of excited atoms) becomes significant enough to lead to a total decrease in the population density. While the effect can be seen for both populations, the $1s_4$ density typically shows the eventual decrease at a higher pressure due to the effects of radiation trapping. Since the only radiative decay channel for resonant level atoms is to the ground state, the VUV (Vacuum Ultraviolet) light that is emitted for this transition is reabsorbed by ground state atoms, repopulating the resonant levels. The amount of ground state atoms increases with pressure, but eventually this radiation trapping reaches a saturation point, and the previously outlined quenching mechanisms take over.¹⁷

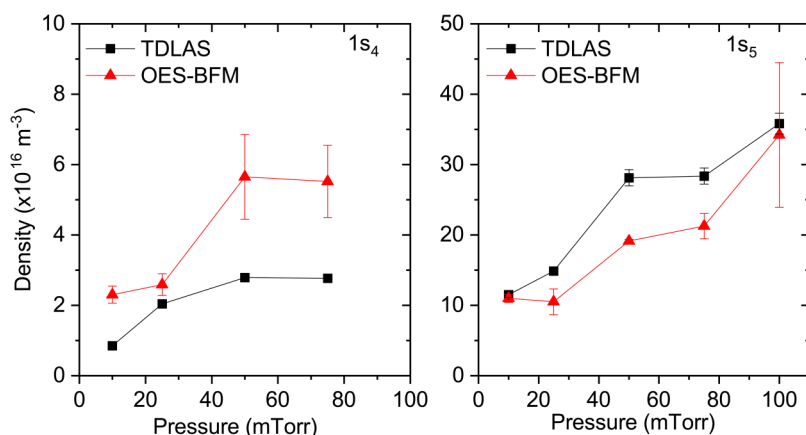


FIG. 6. Density of Ar $1s_4$ and $1s_5$ states vs pressure at 150 W and with no added bias. Solid lines are for visual guidelines.

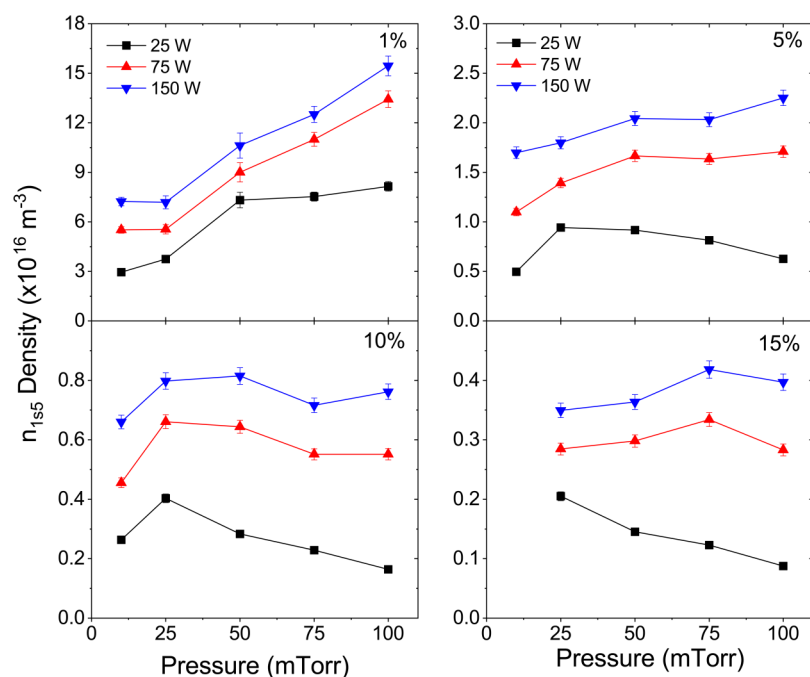


FIG. 7. Ar 1s₅ density measured by TDLAS vs pressure for different concentrations of Cl₂ in Ar with no added bias. Solid lines are for visual guidelines.

The results from TDLAS and OES-BFM in pure Ar, as shown in Fig. 6, show the expected behavior as the discharge pressure is increased. Both measurement techniques show an increase in the 1s₄ density as a function of pressure up to 75 mTorr and begins to saturate. It is important to point out the differences in pressure ranges between this work and that of the known literature. Since most of the cited work operate in an ICP configuration, the pressure ranges are much lower, typically up to 25 mTorr to observe the full effect.^{17,18,40,12} However, the work done by Sushkov *et al.* in a parallel plate CCP has very similar experimental conditions.²² Sushkov shows similar effects at comparable pressures to our work, with an extension that shows the decrease in both the 1s₄ and 1s₅ densities after 75–100 mTorr, the upper pressure limit of this work.

2. Ar/Cl₂ discharge

The relationship between the Ar 1s₅ density and Cl₂ concentration is shown for different rf powers in Fig. 7 as obtained by TDLAS measurements. An increase in concentration accelerates the expected trend of the initial rise, then fall of the density as pressure is increased. This is most evident in the comparison between the 1% and 10% concentrations, as the 1% shows a very similar result as the pure Ar discharge, while the 10% shows a maximum at 25 mTorr, and a decrease as pressure is increased. The results for 25 W power show a much more pronounced fall as pressure is increased past 25 mTorr. This could be due to an increase in the electron density as power is increased, leading to more electron-atom collisions that could sustain the production of metastables.

B. RF power

1. Ar discharge

An increase in the rf power while the pressure remains constant serves to increase the plasma density.¹⁸ While the plasma density, and, therefore, the electron density, is expected to increase, the electron temperature T_e is expected to remain roughly constant as the mean free path of the species in the plasma remains the same. This increase in the plasma density facilitates an increase in the resonant level densities through electron-atom collisions from the ground state, and electron-atom collisions of the metastable levels, forcing a population transfer into the resonant levels. An increase in the metastable level density as a function of power can be expected for many of the same reasons, however to a much lesser extent. There is evidence of an increase of the 1s₅ metastable level with power in the literature, but there are also cases where the density remains constant.^{18,25,22,12} The most analogous literature source to this work, Sushkov, shows an increase and then leveling off of the 1s₅ and 1s₄ densities, although the trend for the metastable level is much less pronounced.²²

In general, the 1s₄ density increases with power at a constant pressure, while the 1s₅ density typically initially increases, then decreases. This is particularly true at lower pressures where the effects of increased pressure, as outlined in Sec. V A, are not as prominent. Figure 8 shows the effect of increasing power on the 1s₄ and 1s₅ densities at 50 mTorr for both TDLAS and OES-BFM measurement techniques. The 1s₄ densities increase with power as measured by TDLAS and OES-BFM, which is expected. Additionally, the similarity in trends for the 1s₅ density is encouraging. Both show a slight yet consistent decrease in the density as the power is increased, and this trend is consistent within all studied pressures.

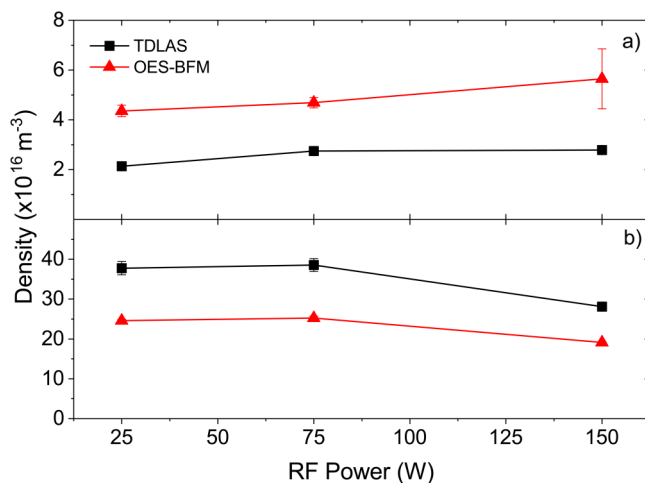


FIG. 8. Density of Ar (a) 1s₄ and (b) 1s₅ densities vs rf power measured with TDLAS and OES-BFM at 50 mTorr with no added bias. Solid lines are for visual guidelines.

2. Ar/Cl₂ discharge

The addition of Cl₂ in the discharge is expected to show an increase in the Ar metastable level density as the rf power is increased.⁴¹ When the rf power is increased, the plasma density, and, therefore, the electron density, will increase, but not necessarily the negative ion density.⁴¹ Low energy electrons are lost to the negative ion formation in an Ar/Cl₂ discharge, while the electron density increases with power. The increase in the electron density facilitates high energy electron collisions with ground state atoms to produce Ar metastables, while the decrease in low energy electrons reduces the amount of metastables that are lost to low energy electron mixing.⁴⁰

Indeed, there is a general increase in the Ar metastable density as the rf power is increased for discharges without added dc bias as shown in Fig. 9. The concentration of Cl₂ added to the discharge does not have a direct effect on the increasing trend of density with power, but it is important to keep in mind that the increase in concentration causes a drastic decrease in the Ar 1s state population, in general. As the Cl₂ concentration is increased, the electron density will decrease to maintain quasineutrality. Increasing the concentration will also cause more low energy electrons to be lost to the creation of negative ions, although this will once again not increase as the power is increased. Although data for only one pressure are shown here, the trend is consistent across the pressure range studied, with higher pressures typically having higher densities.

C. DC bias

The negative dc self-bias that forms on the powered electrode due to the blocking capacitor in the rf power circuit leads to a larger potential drop between the plasma bulk and the powered electrode across the corresponding sheath. In semiconductor processing, this can be an advantage as the substrate can be placed on

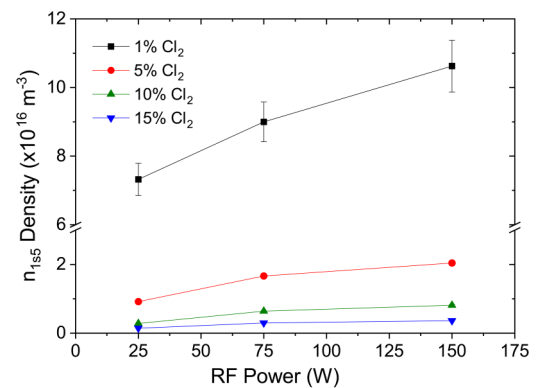


FIG. 9. Ar 1s₅ density measured by TDLAS vs rf power for different concentrations of Cl₂ in an Ar/Cl₂ discharge at 50 mTorr with no added bias. Solid lines are for visual guidelines.

the powered electrode to take advantage of the high ion acceleration energy. In our case however, the goal is to etch a large grounded outer surface. This is not possible without the use of a positive dc bias on the powered electrode due to the asymmetric discharge configuration.⁵ The positive dc bias essentially serves to flip the discharge asymmetry that causes a larger voltage drop between the plasma bulk and the smaller powered electrode, thus making the larger grounded electrode the surface with the largest voltage drop. This leads to larger ion energy and ion flux into the grounded surface and provides the physical energy component of IARIE. Further explanations of the effect of positive dc biasing on etching mechanisms and results can be found in previous work.⁴⁻⁶

The effect of dc biasing on rf CCP etching reactors has been studied by a number of research groups, both experimentally and with particle-in-cell simulations.⁴²⁻⁴⁷ However, a majority of this work was done to study the addition of a negative added bias on either the powered or grounded electrodes, rather than a positively added bias. While these works are useful for gaining a general understanding of the effects of dc bias on the discharge, the complete picture for the purposes of SRF cavity etching remains incomplete. Understanding the relationship between the Ar 1s states, and later T_e and N_e , and total positive dc bias will provide better insight into the effect of dc bias on the plasma dynamics.

1. Ar discharge

The effects of dc bias on the 1s₅ densities can be seen in Fig. 10. The introduction of a positive dc bias causes a decrease in the 1s₅ density, with a larger drop as the pressure is increased. For most cases, increasing the bias has no significant effect on the density, with the exception being when the pressure is higher. Although an increase in 1s₅ density with dc bias is seen for 100 mTorr, the overall increase is rather small. A subtle drop in density can be seen for 75 W and 150 W, particularly for the higher pressures, but the effect is essentially within the statistical error.

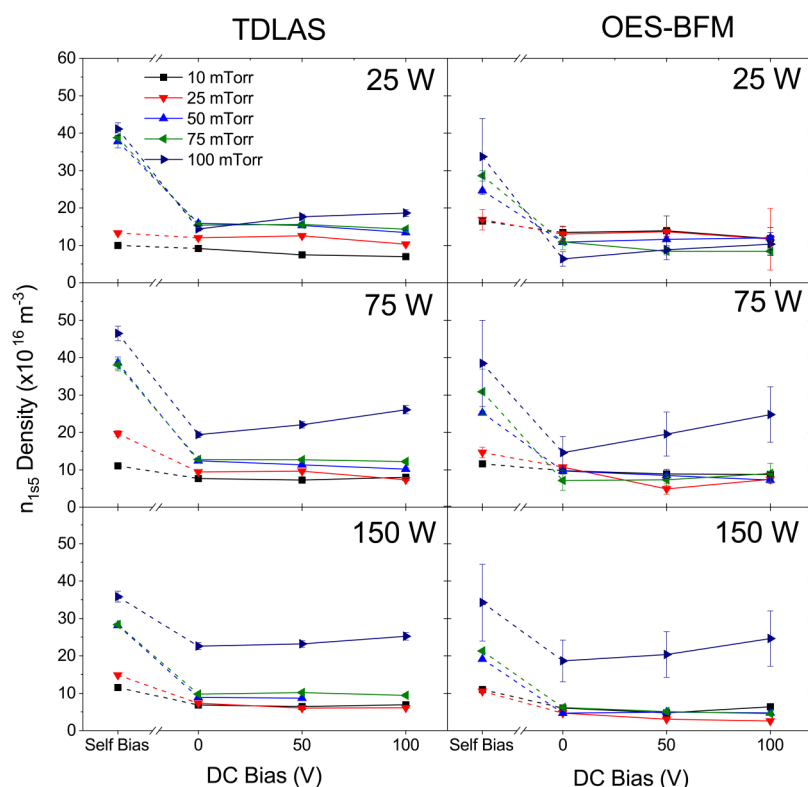


FIG. 10. Ar $1s_5$ density vs dc bias for 25, 75, 150 W power measured with TDLAS and OES-BFM. The dashed lines indicate the negative bias region outlined in Sec. III. Solid/dashed lines are for visual guidelines.

A comparison of TDLAS and OES-BFM for the $1s_4$ densities (not shown) show similar trends as seen in Fig. 10, and results from OES-BFM show an overall drop in density as a positive dc bias is introduced for each $1s$ density (including the $1s_2$ and the $1s_3$ densities). Both measurement techniques show essentially the same trends, including the increase in density with dc bias at higher pressures.

The decrease in the $1s$ densities as positive bias is introduced could be due to an increase in the ionization of these states and a total increase in the plasma density. Indeed, there are multiple studies that show an increase in the ion/electron density as bias becomes more positive.^{46,47} As the powered electrode becomes positively biased, the electron current increases through this surface with an increased energy. This effect was recorded by measuring the current through the dc power supply that provides the positive bias. These electrons then cause high energy secondary electron emission from the powered electrode that can effectively ionize neutral atoms in the discharge. In addition, the larger electric fields in the rf sheath and the bulk result in more forced ionization processes.⁴⁷ The total positive dc biases serve to increase the plasma volume inside the discharge chamber, while total negative biases restrict the discharge to the smaller region between the two electrodes.⁴⁷ The positive bias effectively “pushes” the discharge throughout the chamber as the entire grounded surface (with a much larger surface area) becomes the most attractive surface for ions in the discharge, and the powered electrode becomes the least. This expansion of plasma volume is confirmed qualitatively by the

observation of the discharge as positive bias is added. In addition, a measured increase in the electron current as a positive dc bias is introduced and then increased means that an equal ion current must be flowing through the grounded surface due to the conservation of current.

2. Ar/Cl₂ discharge

In general, the behavior of the Ar $1s_5$ density as a function of bias in Ar/Cl₂ discharges is similar to the relationship outlined in a pure Ar discharge. This is particularly interesting because of the large difference in the densities as the addition of Cl₂ reduces the density by two to three orders of magnitude. However, the relationship between density and dc bias changes as other external parameters, most particularly pressure and power, are varied.

Figure 11 shows the relative Ar $1s_5$ density as a function of dc bias for 25 mTorr and 100 mTorr. The trends for the 25 mTorr set show very similar behavior as in pure Ar as the density drops when a positive bias is introduced and remains relatively constant as the bias is increased. For higher pressures however, it seems that the increase in bias does much less to decrease the density, particularly for higher powers. In addition, the increase in bias also has an effect in increasing the Ar $1s_5$ density, even to the point in which it surpasses the value for self-bias. No explicit explanation for this behavior can be offered at this time, but forthcoming analysis of the electron temperature, electron density, and EEDF will serve to help provide answers.

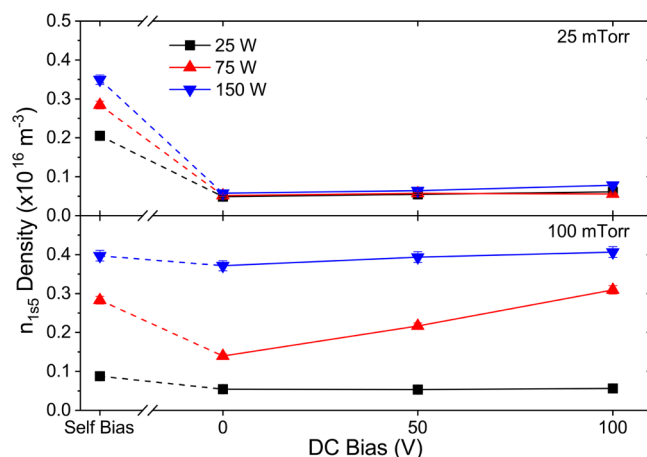


FIG. 11. Ar 1s₅ density measured by TDLAS vs dc bias for 15% Cl₂ in an Ar/Cl₂ discharge. The dashed lines indicate the negative bias region outlined in Sec. III. Solid/dashed lines are for visual guidelines.

D. Cl₂ concentration

The addition of Cl₂ in an Ar discharge adds a great deal of complexity to the kinetics and charge particle balance of the plasma. An Ar/Cl₂ plasma is electronegative, which means that there is an additional negatively charged species, namely, negative Cl ions in this case, in the discharge. However, the quasineutrality condition does not change and the total amount of positive and negative species in the discharge (macroscopically) must be equal. With an additional negative species in the discharge, the amount of electrons will naturally decrease, and, therefore, the amount of

electronic collisions will decrease. In addition, there are a number of new electronic excitation channels involving Cl₂, such as molecular and atomic ionization, dissociative attachment (Cl⁻ formation), and dissociation (molecular splitting).² As previously mentioned in Sec. III B, the Cl collisional quenching rate of Ar metastable and resonant level densities is quite high compared to other commonly used molecular gases in discharges.³⁷ With all of these new processes in mind, it should not be surprising that the Ar 1s₄ and 1s₅ densities are expected to decrease as Cl₂ is added to the discharge. Indeed, there are a number of sources that have shown theoretically and experimentally that this is the case for different types of discharges.^{2,48,49} While the general effect of Cl₂ concentration on the Ar 1s densities is known, the experimental confirmation between this work and outside sources is important. It is also pertinent to study the effects of Cl₂ concentration as it pertains to the other external parameters, particularly dc bias, for etching experiments.

The effect of increasing Cl₂ concentration on the Ar 1s₅ density for different pressures is shown in Fig. 12. In all cases, just a 1% concentration of Cl₂ significantly decreases the Ar metastable density, with an eventual leveling off as the concentration is increased. This relationship matches very closely to previously published work involving the study of Ar metastable density and Cl₂ concentration, as well as relationships established with other molecular gases.^{48,23} The comparison to the work done by Scheller *et al.* is quite intriguing, with the data trend being almost identical.⁴⁸ However, Scheller does show an initial increase in the Ar metastable density at very low concentrations of Cl₂ in Ar.⁴⁸ This increase was not seen for any of the measurements made in this work, but this is most likely due to experimental limitations as very low Cl₂ concentrations (<1%) are required. Scheller explains that the initial increase in metastables at low Cl₂ concentrations is due to a decrease in metastable relaxation as low energy electrons are

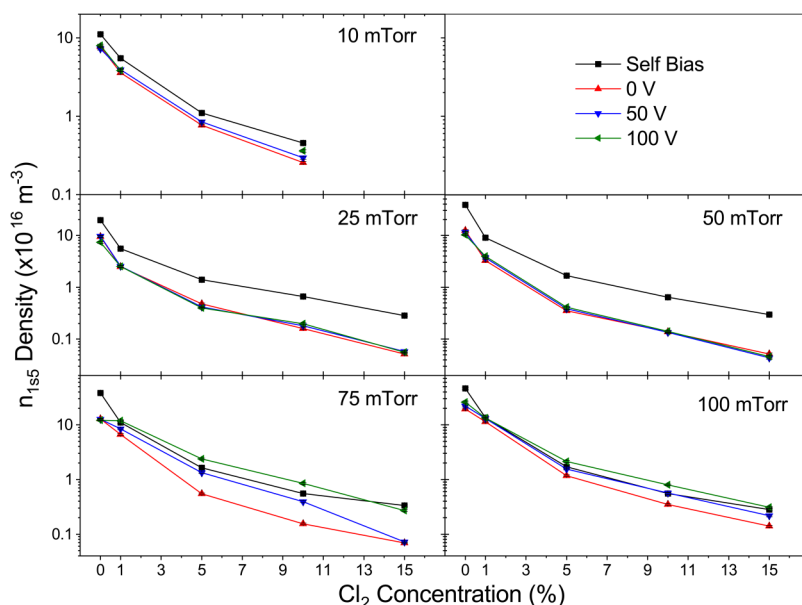


FIG. 12. Ar 1s₅ density measured by TDLAS vs Cl₂ concentration at 75 W. Solid lines are for visual guidelines.

consumed by attachment processes of Cl_2 .⁴⁸ As the concentration increases, the collisional quenching processes quickly become dominant and the Ar $1s_5$ density decreases accordingly.

The amount of Ar metastables that are lost when Cl_2 is added is significant, with a typical drop of two orders of magnitude as the concentration is increased from 0% to 15%. This large drop in Ar metastable density as measured by TDLAS gives additional credence to the limitations of OES-BFM outlined in Sec. III. Typical values of the Ar metastable density at concentrations above 5% are in the $10^{14} - 10^{16} \text{ m}^{-3}$ range, with the larger values attributed to the self-bias results.

VI. DISCUSSION

Among the external parameters studied in this work, the external dc bias is arguably the most important as it is directly related to the effectiveness of the etching of niobium and SRF cavities. In many cases, a negative external bias is added to either electrode to increase the ion energy into that surface and to assist in etching. As the desired surface to be etched is the inside surface of a grounded cylinder, a positive dc bias is added to the powered electrode to flip the natural asymmetry caused by the unequal surface areas and force ions into the grounded surface. When a positive dc bias is added to the powered electrode, the density of all $1s$ states drops significantly but does not necessarily continue to change as bias is increased. Studies conducted on the effect of dc bias have shown that the plasma density increases as the dc bias on the powered electrode becomes more positive.^{43,44,47,46} A drop in Ar $1s$ densities as the plasma density increases is indicative of increased ionization of the $1s$ states and the $2p$ states that populate them. Indeed, preliminary results using a collisional radiative model (CRM) based primarily on the work of Zhu *et al.*^{49,50} show a decrease in the electron temperature and an increase in the electron density as the positive dc bias is introduced.

Figure 13 shows the drop of T_e with the introduction of the positive dc bias calculated using the CRM outlined in the previous paragraph. This indicates that the average thermal electron energy

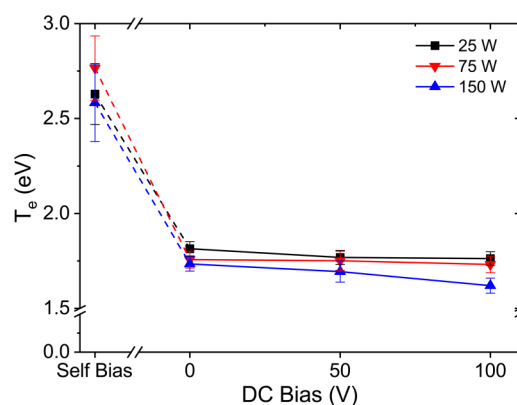


FIG. 13. Electron temperature obtained from CRM vs dc bias in an Ar discharge at 75 mTorr. The dashed lines indicate the negative bias region outlined in Sec. III. Solid/dashed lines are for visual guidelines.

decreases when the positive dc bias is implemented, thus pushing the EEDF toward energies that are more suitable for the ionization of already excited states ($1s$ and $2p$ states). In addition, adding dc bias increases the amount of secondary electrons that are emitted from the powered electrode as electrons are quickly accelerated into the positively biased surface. High energy secondary electrons contribute greatly to the ground state ionization as they traverse the plasma chamber. These secondary electrons are not included in the CRM, so they would have no effect on the thermal electron energy (T_e). Further study of these effects and their consequences is left to future work.

VII. CONCLUSIONS

Two different noninvasive spectroscopy techniques were used to measure the density of the first four excited states of Ar in a coaxial cylindrical rf CCP designed for the plasma processing of SRF cavities. These excited state densities were measured for both Ar and Ar/ Cl_2 mixtures of varying concentrations as the Ar/ Cl_2 mixture is necessary for etching of these cavities. The two measurement techniques, TDLAS and OES-BFM, were conducted in tandem as pertinent external parameters were varied to develop a working model to describe this particular discharge. While TDLAS is a much more accurate measurement technique, it requires the use of a tunable diode laser. In addition, TDLAS can only measure one density at a time as it requires the laser to be tuned to a specific atomic transition. OES-BFM has gained popularity since its introduction by Schulze *et al.*¹² and further implementation by Boffard *et al.*¹⁷ This optical method is advantageous due to its ability to measure all four Ar $1s$ state densities simultaneously using inexpensive low-resolution spectroscopy systems. Similar to the TDLAS method, OES-BFM avoids any requirement that knowledge of the EEDF must be known *a priori* as the method does not require the use of any collisional cross sections. However, this method is not nearly as accurate as TDLAS and the use of a low-resolution spectrometer in favor of speed can be a detriment when using a variety of strong and weak lines in the analysis. In addition, OES-BFM is limited in its ability to measure these densities for multigas discharges, especially when Cl_2 is involved, due to much lower excited state densities and much higher photon escape factors.

As a direct comparison, TDLAS is much more effective than OES-BFM at measuring the excited state density with accuracy and consistency. The results of this work show agreement between the two methods up to a factor of three for the vast majority of the external parameters studied, which is consistent with other studies.^{17,22,32,23} At a minimum, OES-BFM is effective in modeling qualitative relationships between the excited state density and the external parameters, especially in regard to pressure and dc bias. This can be quite useful to gain a quick yet effective understanding of a discharge.

ACKNOWLEDGMENTS

This work was supported by the Department of Energy (DOE) under Grant No. DE-SC0014397. The authors would like to give a special thanks to Forrest Miller for his invaluable help with writing the analysis software.

REFERENCES

- ¹H. R. Koenig and L. I. Maissel, "Application of rf discharges to sputtering," *IBM J. Res. Dev.* **14**, 168–171 (1970).
- ²N. L. Bassett and D. J. Economou, "Effect of Cl₂ additions to an argon glow discharge," *J. Appl. Phys.* **75**, 1931–1939 (1994).
- ³J. Upadhyay, S. Popović, L. Vusković, D. Im, A.-M. Valente, and H. Phillips, "Plasma processing of large surfaces with application to SRF cavity modification," Technical Report (Thomas Jefferson National Accelerator Facility, Newport News, VA, 2013).
- ⁴J. Upadhyay, D. Im, S. Popović, A.-M. Valente-Feliciano, L. Phillips, and L. Vusković, "Plasma processing of large curved surfaces for superconducting rf cavity modification," *Phys. Rev. Spec. Top.-Accelerators Beams* **17**, 122001 (2014).
- ⁵J. Upadhyay, D. Im, S. Popović, A.-M. Valente-Feliciano, L. Phillips, and L. Vusković, "Etching mechanism of niobium in coaxial Ar/Cl₂ radio frequency plasma," *J. Appl. Phys.* **117**, 113301 (2015).
- ⁶J. Upadhyay, D. Im, S. Popović, L. Vusković, A.-M. Valente-Feliciano, and L. Phillips, "Reversal of the asymmetry in a cylindrical coaxial capacitively coupled Ar/Cl₂ plasma," *J. Vac. Sci. Technol. A* **33**, 061309 (2015).
- ⁷J. Upadhyay, J. Peshl, S. Popović, A.-M. Valente-Feliciano, and L. Vusković, "Effect of self-bias on cylindrical capacitive discharge for processing of inner walls of tubular structures—Case of SRF cavities," *AIP Adv.* **8**, 085008 (2018).
- ⁸J. Upadhyay, D. Im, J. Peshl, M. Băsović, S. Popović, A.-M. Valente-Feliciano, L. Phillips, and L. Vusković, "Apparatus and method for plasma processing of SRF cavities," *Nucl. Instrum. Methods Phys. Res. A* **818**, 76–81 (2016).
- ⁹J. Upadhyay, A. Palczewski, S. Popović, A.-M. Valente-Feliciano, D. Im, H. Phillips, and L. Vusković, "Cryogenic rf test of the first SRF cavity etched in an rf Ar/Cl₂ plasma," *AIP Adv.* **7**, 125016 (2017).
- ¹⁰P. Kneisel, "Cavity preparation/assembly techniques and impact on q-realistic q-factors in a module: Review of modules," *Nucl. Instrum. Methods Phys. Res. A* **557**, 250–258 (2006).
- ¹¹A. J. L. Michael and A. Lieberman, *Principles of Plasma Discharges and Materials Processing* (John Wiley & Sons Inc., 1994).
- ¹²M. Schulze, A. Yanguas-Gil, A. von Keudell, and P. Awakowicz, "A robust method to measure metastable and resonant state densities from emission spectra in argon and argon-diluted low pressure plasmas," *J. Phys. D Appl. Phys.* **41**, 065206 (2008).
- ¹³J. B. Boffard, G. A. Piech, M. F. Gehrke, L. Anderson, and C. C. Lin, "Measurement of electron-impact excitation cross sections out of metastable levels of argon and comparison with ground-state excitation," *Phys. Rev. A* **59**, 2749 (1999).
- ¹⁴J. B. Boffard, C. C. Lin, and C. A. DeJoseph, Jr., "Application of excitation cross sections to optical plasma diagnostics," *J. Phys. D Appl. Phys.* **37**, R143 (2004).
- ¹⁵J. B. Boffard, B. Chiaro, T. Weber, and C. C. Lin, "Electron-impact excitation of argon: Optical emission cross sections in the range of 300–2500 nm," *At. Data Nucl. Data Tables* **93**, 831–863 (2007).
- ¹⁶J. B. Boffard, R. Jung, L. Anderson, and C. Lin, "Electron-impact excitation of rare-gas atoms from the ground level and metastable levels," *Adv. At. Mol. Opt. Phys.* **54**, 320 (2007).
- ¹⁷J. B. Boffard, R. Jung, C. C. Lin, and A. Wendt, "Measurement of metastable and resonance level densities in rare-gas plasmas by optical emission spectroscopy," *Plasma Sources Sci. Technol.* **18**, 035017 (2009).
- ¹⁸J. B. Boffard, R. Jung, C. C. Lin, and A. Wendt, "Optical emission measurements of electron energy distributions in low-pressure argon inductively coupled plasmas," *Plasma Sources Sci. Technol.* **19**, 065001 (2010).
- ¹⁹J. B. Boffard, R. Jung, C. C. Lin, L. Aneskevich, and A. Wendt, "Optical diagnostics for characterization of electron energy distributions: Argon inductively coupled plasmas," *Plasma Sources Sci. Technol.* **20**, 055006 (2011).
- ²⁰J. B. Boffard, R. Jung, C. C. Lin, L. Aneskevich, and A. Wendt, "Argon 420.1–419.8 nm emission line ratio for measuring plasma effective electron temperatures," *J. Phys. D Appl. Phys.* **45**, 045201 (2012).
- ²¹S. Siepa, S. Danko, T. V. Tsankov, T. Mussenbrock, and U. Czarnetzki, "On the OES line-ratio technique in argon and argon-containing plasmas," *J. Phys. D Appl. Phys.* **47**, 445201 (2014).
- ²²V. P. Sushkov, H. T. Do, and R. Hippler, "Application of the escape factor method for determination of excited states densities in a low-pressure argon radio-frequency discharge," *Contrib. Plasma Phys.* **53**, 549–559 (2013).
- ²³M. Fiebrandt, B. Hillebrand, S. Spiekermeier, N. Bibinov, M. Böke, and P. Awakowicz, "Measurement of Ar resonance and metastable level number densities in argon containing plasmas," *J. Phys. D Appl. Phys.* **50**, 355202 (2017).
- ²⁴N. Beverini, G. Cicconi, G. L. Genovesi, and E. Piano, "Metastable level density and temperature measurement in a low-density argon plasma," *Plasma Sources Sci. Technol.* **6**, 185–188 (1997).
- ²⁵S. Schröter, H. Bahre, M. Böke, and J. Winter, "The role of argon metastables in an inductively coupled plasma for treatment of PET," *Plasma Process. Polym.* **11**, 239–246 (2014).
- ²⁶T. Holstein, "Imprisonment of resonance radiation in gases," *Phys. Rev.* **72**, 1212–1233 (1947).
- ²⁷R. McWhirter, in *Plasma Diagnostic Techniques*, edited by R. H. Huddleston and S. L. Leonard (Academic Press, New York, 1965), p. 201.
- ²⁸Y. Golubovskii, S. Gorchakov, and D. Uhrlandt, "Transport mechanisms of metastable and resonance atoms in a gas discharge plasma," *Plasma Sources Sci. Technol.* **22**, 023001 (2013).
- ²⁹X.-M. Zhu, Z.-W. Cheng, Y.-K. Pu, and U. Czarnetzki, "Escape factors for Paschen 2p–1s emission lines in low-temperature Ar, Kr, and Xe plasmas," *J. Phys. D Appl. Phys.* **49**, 225204 (2016).
- ³⁰R. Mewe, "Relative intensity of helium spectral lines as a function of electron temperature and density," *Br. J. Appl. Phys.* **18**, 107–118 (1967).
- ³¹R. Mewe, "Simplified model for ionization and recombination in a hydrogenic plasma with resonance radiation trapping," *Z. Naturforsch. A* **25**, 1798–1803 (1970).
- ³²J. Li, F.-X. Liu, X.-M. Zhu, and Y.-K. Pu, "The spatially resolved measurements of the atomic densities in argon Paschen 1s levels by OES in a capacitively coupled plasma," *J. Phys. D Appl. Phys.* **44**, 292001 (2011).
- ³³S. Hübner, N. Sadeghi, E. A. D. Carbone, and J. J. A. M van der Mullen, "Density of atoms in Ar*(3p54s) states and gas temperatures in an argon surfatron plasma measured by tunable laser spectroscopy," *J. Appl. Phys.* **113**, 143306 (2013).
- ³⁴A. Kramida, Y. Ralchenko, and Ju. Reader, and NIST ASD Team NIST Atomic Spectra Database (ver. 5.6.1) [Online]. Available: <https://physics.nist.gov/asd> [2019 May 31]. National Institute of Standards and Technology, Gaithersburg, MD (2018).
- ³⁵K. Liu and M. G. Littman, "Novel geometry for single-mode scanning of tunable lasers," *Opt. Lett.* **6**, 117–118 (1981).
- ³⁶S. C. Doret, "Simple, low-noise piezo driver with feed-forward for broad tuning of external cavity diode lasers," *Rev. Sci. Instrum.* **89**, 023102 (2018).
- ³⁷J. E. Velazco, J. H. Kolts and D. W. Setser, "Rate constants and quenching mechanisms for the metastable states of argon, krypton, and xenon," *J. Chem. Phys.* **69**, 4357–4373 (1978).
- ³⁸S. Wang, A. E. Wendt, J. B. Boffard, C. C. Lin, S. Radovanov, and H. Persing, "Noninvasive, real-time measurements of plasma parameters via optical emission spectroscopy," *J. Vac. Sci. Technol. A* **31**, 021303 (2013).
- ³⁹V. M. Donnelly and M. V. Malyshev, "Diagnostics of inductively coupled chlorine plasmas: Measurements of the neutral gas temperature," *Appl. Phys. Lett.* **77**, 2467–2469 (2000).
- ⁴⁰G. A. Hebner and P. A. Miller, "Behavior of excited argon atoms in inductively driven plasmas," *J. Appl. Phys.* **87**, 8304–8315 (2000).
- ⁴¹C. B. Fleddermann and G. A. Hebner, "Negative ion densities in chlorine- and boron trichloride-containing inductively coupled plasmas," *J. Vac. Sci. Technol. A* **15**, 1955–1962 (1997).
- ⁴²M. A. Lieberman and S. E. Savas, "Bias voltage in finite length, cylindrical and coaxial radio-frequency discharges," *J. Vac. Sci. Technol. A* **8**, 1632–1641 (1990).
- ⁴³E. Kawamura, M. A. Lieberman, A. J. Lichtenberg, and E. A. Hudson, "Capacitive discharges driven by combined dc/rf sources," *J. Vac. Sci. Technol. A* **25**, 1456–1474 (2007).

- ⁴⁴E. Kawamura, A. J. Lichtenberg, and M. A. Lieberman, "Secondary electrons in rf and dc/rf capacitive discharges," *Plasma Sources Sci. Technol.* **17**, 045002 (2008).
- ⁴⁵P. Diomede, S. Longo, D. J. Economou, and M. Capitelli, "Hybrid simulation of a dc-enhanced radio-frequency capacitive discharge in hydrogen," *J. Phys. D Appl. Phys.* **45**, 175204 (2012).
- ⁴⁶P. Diomede, D. Kim, and D. J. Economou, "Particle-in-cell simulation of electron and ion energy distributions in dc/rf hybrid capacitively-coupled plasmas," *AIChE J.* **59**, 3214–3222 (2013).
- ⁴⁷M. Zeuner, H. Neumann, and J. Meichsner, "Ion energy distributions in a dc biased rf discharge," *J. Appl. Phys.* **81**, 2985–2994 (1997).
- ⁴⁸G. R. Scheller, R. A. Gottscho, T. Intrator, and D. B. Graves, "Nonlinear excitation and dissociation kinetics in discharges through mixtures of rare and attaching gases," *J. Appl. Phys.* **64**, 4384–4397 (1988).
- ⁴⁹X.-M. Zhu and Y.-K. Pu, "Optical emission spectroscopy in low-temperature plasmas containing argon and nitrogen: Determination of the electron temperature and density by the line-ratio method," *J. Phys. D Appl. Phys.* **43**, 403001 (2010).
- ⁵⁰X.-M. Zhu, Z.-W. Cheng, E. Carbone, Y.-K. Pu, and U. Czarnetzki, "Determination of state-to-state electron-impact rate coefficients between Ar excited states: A review of combined diagnostic experiments in afterglow plasmas," *Plasma Sources Sci. Technol.* **25**, 043003 (2016).